11th International Symposium on Turbulence and Shear Flow Phenomena (TSFP11)
Southampton, UK, July 30 to August 2, 2019

TURBULENT SHEAR FLOW IN SYMMETRIC SPATIAL SUBMERGED HYDRAULIC JUMP

Vimaldoss Jesudhas
Department of Civil & Environmental Engg.
University of Windsor
401, Sunset Ave, Windsor, ON, Canada
jesudha@uwindsor.ca

Ram Balachandar
Department of Civil & Environmental Engg.
University of Windsor
401, Sunset Ave, Windsor, ON, Canada
rambala@uwindsor.ca

Tirupati Bolisetti
Department of Civil & Environmental Engg
University of Windsor
401, Sunset Ave, Windsor, ON, Canada
tirupati@uwindsor.ca

ABSTRACT

Spatial or three-dimensional hydraulic jumps are often encountered in hydraulic engineering when a conduit opens into a rectangular channel or in expanding stilling basins. The present paper aims to explore the three-dimensional turbulent features of a symmetric spatial hydraulic jump. To this end, an unsteady, Improved Delayed Detached Eddy Simulation of the flow field is carried out at a jet exit Reynolds number of 3.3 x 10^4. A brief description of the mean flow field is presented. The instantaneous flow field are further analysed and presented with pertinent discussions. Vortex identification techniques were used to qualitatively describe the coherent structures in the flow. The results of the analysis are presented with appropriate discussions.

INTRODUCTION

Hydraulic Jumps are very commonly encountered in hydraulic engineering practice. They have received significant attention by the researchers due to their practical application as energy dissipators. However most of these studies are focussed on classical and submerged hydraulic jumps which are nominally two-dimensional (2D) in nature. Spatial or three-dimensional (3D) hydraulic jumps are formed when a conduit opens into a rectangular channel (low-head dams), expanding stilling basins or when one of the sluice gates is opened in a multi-gate system. The different non-dimensional parameters that control the flow characteristics in a spatial hydraulic jump has been documented by Ohtsu et al. (1999). If the tailwater depth d_2 d_2 is higher than the subcritical sequent depth $d_2^*$of a classical hydraulic jump for the given Froude number $F_1 = U_1 / \sqrt{g d_1}$, where U_1 and d_1 are the velocity and flow depth at the conduit outlet, a Submerged Spatial Hydraulic Jump (SSHJ) is formed. At low tailwater depth, the SSHJ flow field will be oscillatory. However, the flow stabilizes itself when the submergence is sufficiently high and the jump becomes symmetric (Zare and Baddour, 2007). The schematic of the typical flow field of a SSHJ is shown in Fig. 1 (adopted from Jesudhas et al., 2019) to show the different flow regions. The complete description of the symmetric SSHJ flow field is provided in Zare and Baddour (2007), Jesudhas et al., (2017 & 2019) and hence not repeated here for brevity.

Studies on the spatial hydraulic jumps are relatively sparse compared to 2D hydraulic jumps. While experimental studies have acquired measurements in spatial locations or planes, the complete 3D flow field is not available for analysis. Numerical analysis could be used to fill the gaps in experimental data to further charactersitize the internal structure of turbulence in SSHJ. To this end, a symmetric SSHJ at 3.3 x 10^4 is simulated using a 3D, unsteady, Improved Delayed Detached Simulation (IDDES). This paper presents the flow structures that were captured in the highly sheared regions of the flow field.

Computational model and validation

The IDDES model is a hybrid RANS-LES approach to turbulence modelling. It uses RANS model near the walls and LES away from it. It is less computationally expensive than a complete LES and captures the large - eddies in the region of interest (shear layer). Shear Stress Transport (SST) k-ω RANS model was used in the present simulation. The free surface deformations were captured using Volume of Fluid (VOF) multiphase model with High-Resolution Interface Capture (HRIC). A detailed formulation of the models used in the simulation is presented in Jesudhas (2016) and hence not presented here. The simulation domain was modelled based on the experiments of Zare and Baddour (2007) to enable comparison. The mesh consists of about 3.5 million hexahedral cells. The IDDES model uses a mesh-dependent blending function to switch between the LES and RANS regions. The mesh was controlled decisively to ensure that LES was performed in the region of interest (shear layer). The complete details of the domain and the mesh is presented in Jesudhas et al. (2019). The simulation was run with a time step of 1 ms and the solution were considered to be converged when the residuals fell below 10^{-6}.

An exhaustive validation of the results including the features of the free surface, velocity, turbulence characteristics and non-dimensional parameters was carried out using AIAA guidelines for Verification and Validation of Computational

Fluids Dynamics (2002). This procedure along with a detailed description of the mean characteristics of the flow are presented in Jesudhas et al. (2017 & 2019). A brief overview of the mean flow characteristics is described in the present paper for the benefit of the reader. However, the present paper aims to enhance the understanding of spatial SSHJ with new analysis and discussions.

RESULTS AND DISCUSSION

Mean Characteristics

Fig. 2 (a-c) presents the mean velocity vectors in three *x-y* (vertical) planes. The $z/B = 0$ plane is the central plane and the $z/B = 0.35$ plane is close to the wall as shown in Fig. 1. The emerging wall-jet flow from the sluice is clearly visible in Fig. 2a as the region of high-velocity. The negative flow region indicated by the negative vectors represents the jump roller. A shear layer is formed between the jump roller and the emerging wall jet. From Fig. 2 it is apparent that the negative flow region extends further downwards as we move from the center to the side walls due to the absence of the wall jet. This can potentially enhance the scour close to the side walls (Pagliara et al., 2009; Jesudhas et al., 2019). Fig. 2(d-e) presents the contours of mean Reynolds stress at the same three *x-y* (vertical) planes. As expected, the mean Reynolds shear stress is maximum in the shear layer between the jump roller and the wall jet in the central plane (Fig. 2d). The mean Reynolds stress decreases as we move towards the side walls due to the decrease in the intensity of the wall-jet flow.

Fig. 3 (a-c) presents the mean velocity vectors in three *x-z* (longitudinal) planes. The plane $y/d_2 = 0.30$ is slightly above the emerging wall jet and the plane $y/d_2 = 0.85$ is closest to the free surface as depicted in Fig. 1. It must be also noted, that due to symmetric nature of the flow field only one half of the domain is presented. The emerging wall-jet flow can be seen as the region of high velocity in Fig. 3a. The separation rollers are formed along the sides of the wall jet. The interaction between the wall jet, jump roller and the separation roller results in a complex three-dimensional shear layer (Jesudhas et al., 2019). The mean Reynolds shear stress is maximum in the plane closest to the emerging wall jet and decreases in intensity as we move towards the free surface due to the expansion of the wall-jet flow (as seen in Figs. 3d-f).

Instantaneous Flow Features

The instantaneous streamwise velocity contours in a horizontal (*x-z*) plane located at $y/d_2 = 0.11$ for two different time instances are presented in Figs. 4a & 4b. This plane cuts through the wall jet at mid-plane. As expected for the prevailing Froude number, the flow field is reasonably symmetrical. The separation rollers at the sides of the wall jet are also shown by the velocity vectors superimposed on the contours. The size of the separation rollers is similar on both sides of the wall jet. The instantaneous streamwise velocity contours in the central plane ($z/B = 0$) of the symmetric SSHJ is presented in Figs. 4c & 4d. As indicated earlier, the free surface height at $t = 30$s is higher than the free surface height at $t = 40$s. Examining the contours and the superimposed velocity vectors in Figs. 4c & 4d, it is clear that the jump roller is well formed at $t = 30$s. This can be seen by the large negative flow region near the free surface in Fig. 4c. The roller is not as well defined at $t = 40$s (Fig. 4d). In Fig. 4c, the large negative flow region near the free surface causes a reduction in the positive velocity region between $0 < x/d_2 < 2$. By continuity considerations, the flow depth is increased at t = 30s. This low frequency oscillatory behavior of the free surface needs to be investigated further.

To analyze the periodic vortex shedding from the conduit opening, the time series of pressure was acquired at specific spatial locations. The frequency of vortex shedding was obtained using an FFT analysis. The corresponding period *T* of vortex shedding is split into four-time instants and the contours of instantaneous vorticity in horizontal (*x-z*) and vertical (*x-y*) planes across the flow field were analyzed. Figs. 5a – 5d show the instantaneous contours of z-vorticity in the central plane ($z/B = 0$) at various time instants. At time $t = T/4$, the periphery of the jet is indicated by a zone of high vorticity (red colour), which evolves with increasing streamwise distance and a fluid structure 'A' is formed (at $x/d_2 = 1.1$). As the structure 'A' is shed and convects downstream, it is it split into smaller vortical structures 'B' and 'C' by the action of the jump roller ($t = 3T/4$, Fig. 5c). The interaction of the wall jet with the bed results in counter-rotating fluid structures near the bed as indicated by the strong negative z-vorticity (blue colour). The smaller structure 'C' convects towards the bed where it interacts with the near bed structures to be broken down further. The interaction of a previously shed vortical structure with the bed is marked in Fig. 5c (at $x/d_2 = 3$). The smaller structure 'B' is carried by the jump roller and is broken down further ($t = 4T/4$, Fig. 5d). Also, plotted in Figs. 5e – 5h is the contours of *y*-vorticity in *x-z* plane located at $y/d_2 = 0.22$ for the corresponding time steps. The periphery of the emanating jet in Figs. 5e – 5h is indicated by the zones of high intensity counter-rotating (red and blue) *y*-vorticity. At time $t = T/4$, one of the legs of a 3D vortical structure is detached (marked by dashed circle in Fig. 5e), while the other remains attached. This indicates that even though the wall-jet type flow is symmetrical, there exists mild fluttering in the lateral direction. As the 3D structure is shed, it is immediately broken down into smaller structures (dashed circle in Fig. 5f) in the region between the jump roller and the wall jet (at $x/d_2 = 1.8$). This makes it difficult to correlate the tracking of structures between the central plane and the mid-jet plane. The smaller counter rotating flow structures (indicated by red and blue) interact with each other (dashed circles in Figs. 5g – 5h), resulting in further breakdown of the structures. All the contours in Fig. 1 collectively indicate that there is the formation of three-dimensional fluid structures which are large to begin with and breakdown with increasing downstream distance.

While turbulence can be quantified by adopting a statistical approach, the structural approach is helpful in identifying organized structures that characterizes the flow field. Moreover, understanding the dynamics of these coherent structures clarifies the energy dissipation in SSHJ. The coherent structures in the symmetric SSHJ flow field were educed using the λ_2 criterion (Jeong and Hussain, 1995). Fig. 6 shows the instantaneous iso-surface for $\lambda_2 = -10$ colored by the contours of instantaneous x-velocity. Also, super-imposed in Fig. 6 are the instantaneous streamlines of velocity (white color). The rectangular vortex rings shed from the conduit opening are enlarged in the inset of Fig. 6 for clarity. These rectangular vortex rings stretch and tend to deform into a circular shape as they move downstream of the conduit opening. The ring deformation is caused by the velocity-pressure differential between the edges and faces of the rectangular vortex ring (Ghasemi et al., 2016). The velocity differential along the edges of the vortex rings can be observed in Fig. 6. As the bed restricts the motion of the rectangular vortex ring in the bottom, the stretching and deformation happens mostly along the sides and the top of the rectangular vortex ring. As the vortex ring moves further downstream, it encounters the reverse flowing rollers (marked in Fig. 6). The interaction between the rollers and the wall-jet causes the vortex rings to break-down to smaller vortex worms. This breakdown of large-scale structures within the roller region is a characteristic feature of hydraulic jumps resulting in energy dissipation.

CONCLUSIONS

The paper presented the results of a three-dimensional, unsteady, improved delayed detached eddy simulation of a symmetric spatial submerged hydraulic jump. The mean flow features of the symmetric spatial submerged hydraulic jump were predicted accurately. Analysis of the instantaneous flow features revealed the presence of periodic vortex shedding from the conduit opening. The large-scale rectangular vortex rings that are formed at the conduct opening evolve into a more circular shape due to the velocity-pressure differential between the edges and faces of the rectangular vortex ring. These large-scale vortex rings are further broken down in smaller-scale vortex worms in the shear layer, resulting in turbulent dissipation of energy.

REFERENCES

AIAA Standards Committee., 2002, *AIAA Guide for the Verification and Validation of Computational Fluid Dynamics Simuations* (G-077-1998).

Ghasemi, A., Roussinova, V., Barron, R. M., and Balachandar, R., 2016, “Large eddy simulation of the near-field vortex dynamics in starting square jet transitioning into steady state“, *Physics of Fluids*, Vol. 28(8), 085104.

Jeong, J., & Hussain, F., 1995, "On the identification of a vortex", *Journal of Fluid Mechanics*, Vol. 285, 69-94.

Jesudhas, V., 2016, *Modeling of free-surface flows with air entrainment*, Doctoral dissertation, University of Windsor, Canada.

Jesudhas, V., Balachandar, R., and Bolisetti, T., 2017, "CFD study of a Spatial Submerged Hydraulic Jump", *Proceedings of the 37th IAHR World Congress,* 13th – 18th August, Kuala Lampur, Malaysia.

Jesudhas, V., Balachandar, R., and Bolisetti, T., 2019, "Numerical Study of a Symmetric Submerged Spatial Hydraulic Jump", *Journal of Hydraulic Research* - (published online).

Ohtsu, I., Yasuda, Y., and Ishikawa, M., 1999, "Submerged hydraulic jumps below abrupt expansions", *Journal of Hydraulic Engineering*, Vol. 125(5), pp. 492 – 499.

Pagliara, S., Palermo, M., and Carnacina, I., 2009, “Scour and hydraulic jump downstream of block ramps in expanding stilling basins”, *Journal of Hydraulic Research*, Vol. 47(4), 503-511.

Zare, H. K., & Baddour, R. E., 2007, "Three-dimensional study of spatial submerged hydraulic jump", *Canadian Journal of Civil Engineering*, Vol. 34(9), pp. 1140 – 1148.

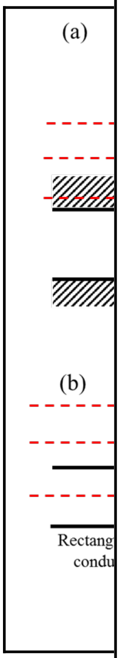

Figure1. Schematic of the typical SSHJ flow field depicting the different flow regions (a) side view (b) plan view (adopted from Jesudhas et al., 2019)

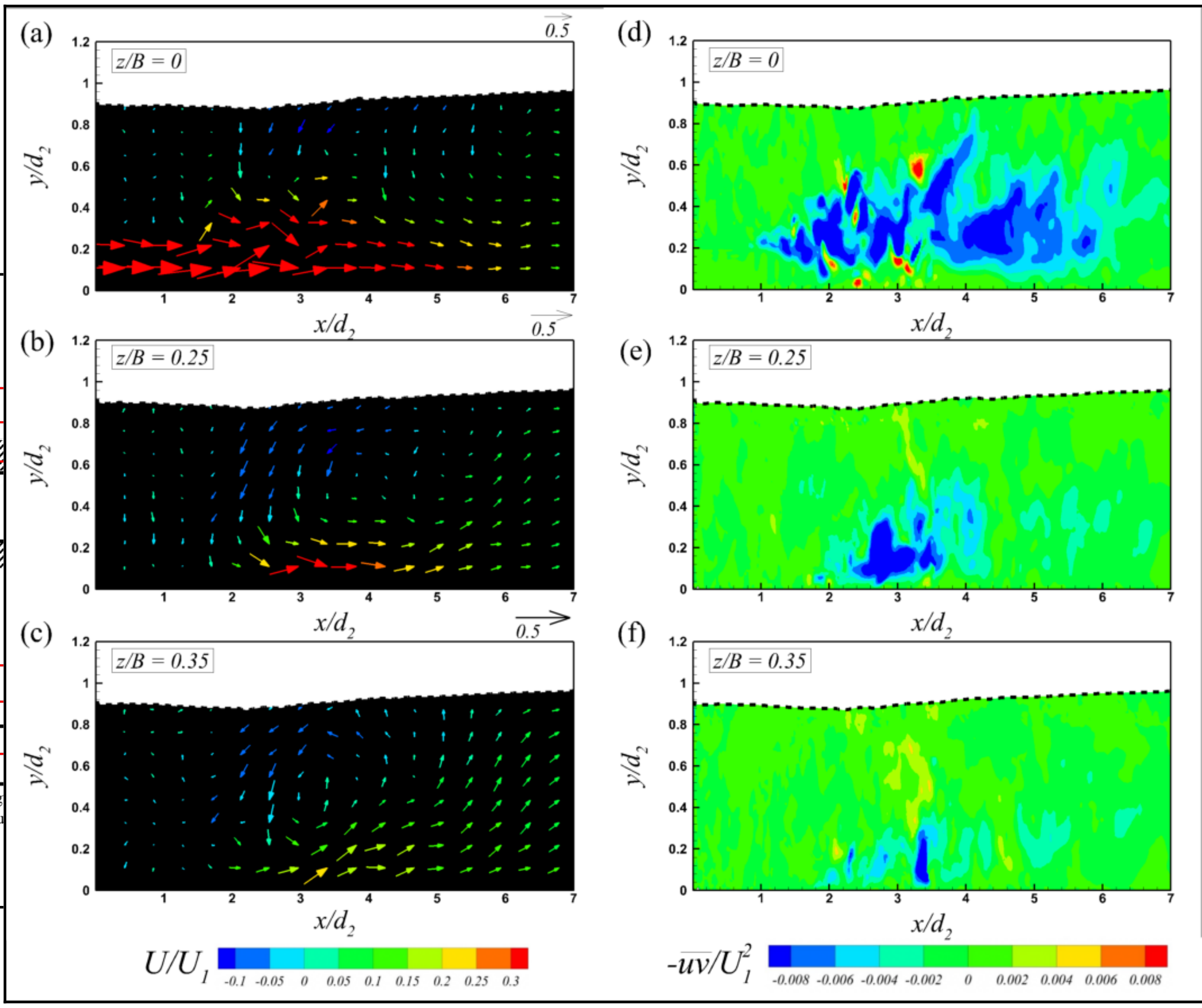

Figure 2. (a-c) Mean velocity vectors (d-f) Mean Reynolds shear stress in three *x-y* planes

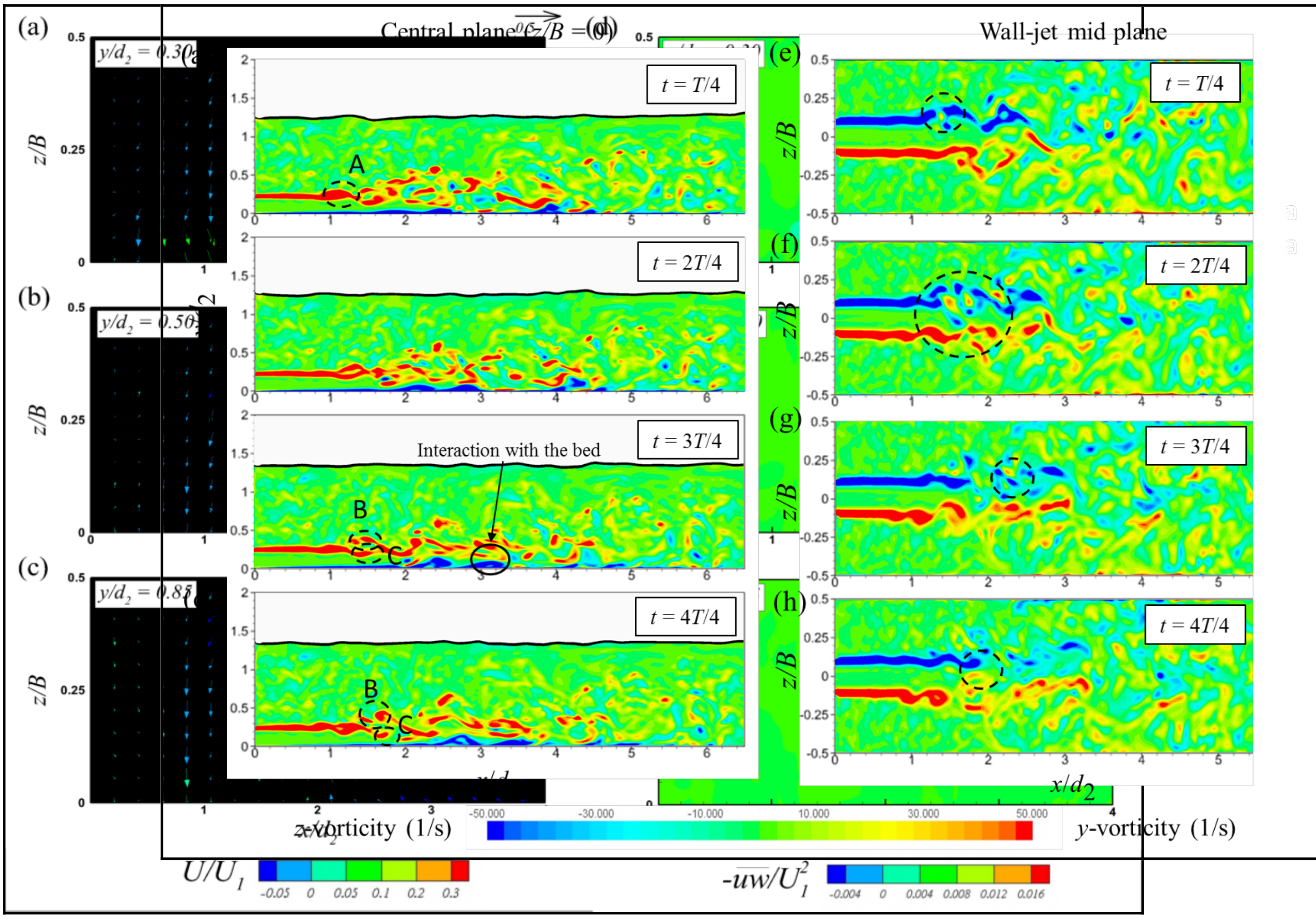

Figure 3. (a-c)

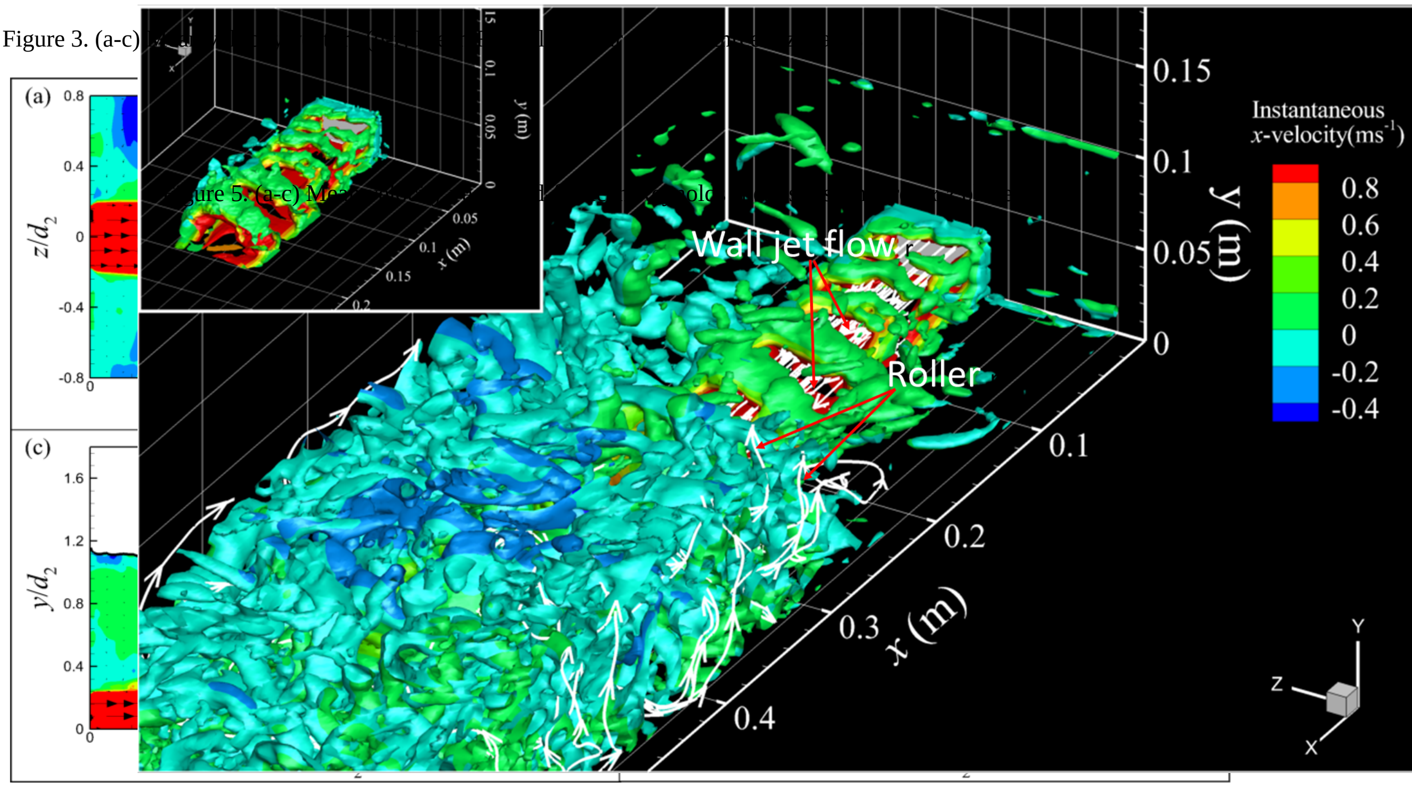

Figure 4. Contours of Instantaneous streamwise velocity

Figure 6. Coherent structures in SSHJ flow field